

**Sodium ion self-diffusion in molten NaBr probed over different length scales**F. Demmel \**ISIS Facility, Rutherford Appleton Laboratory, Didcot, OX11 0QX, United Kingdom*

(Received 18 February 2020; accepted 20 May 2020; published 8 June 2020)

The single-particle dynamics of sodium ions in molten sodium bromide has been investigated with quasielastic neutron scattering. A detailed and rather extensive data analysis procedure allowed determination of the pure sodium ion dynamics with increasing wave vector. Two different evaluation procedures agree perfectly on the resulting diffusion coefficient of sodium ions on long distances. A simple kinetic theory based on binary collisions of hard spheres is not able to reproduce the sodium diffusion coefficient. The derived reduced linewidth from modeling with a Lorentzian spectral function decreases with increasing wave vector towards the first structure factor maximum. That deviation from the hydrodynamic behavior signals the hindrance of the microscopic diffusion process due to the so-called cage effect when microscopic length scales are probed in a dense fluid. The observed quadratic wave-number-dependent decrease might be evidence for a coupling to density fluctuations as the source of the changes in the diffusion process. The results indicate that in the molten salt NaBr near the melting point the self-diffusion process might be governed by similar processes as already observed in dense metallic liquids.

DOI: [10.1103/PhysRevE.101.062603](https://doi.org/10.1103/PhysRevE.101.062603)**I. INTRODUCTION**

Diffusion is a mass transport process occurring in solids, liquids, and gases. Materials science and life as well rely on displacements of atoms and molecules due to thermal motion. According to Fick's law the driving force for diffusion is a concentration gradient [1]. This is also the basic principle for the macroscopic measurements of diffusion coefficients, where tracer techniques are applied to determine diffusion coefficients.

On long length scales, in the hydrodynamic regime, self-diffusion is represented by a partial differential equation for the tagged particle density  $n(r, t)$  (see, for example, Ref. [2]):

$$\frac{\partial n(r, t)}{\partial t} = D \nabla^2 n(r, t). \quad (1)$$

Herein the diffusion coefficient  $D$  appears, which is assumed to be a constant within this derivation. The solution of this equation is a Gaussian spatial distribution  $n(r, t) = \frac{1}{(4\pi Dt)^{3/2}} \exp(-r^2/4Dt)$ , which describes the probability to find a particle after time  $t$  in a distance  $r$  when the particle was at  $t = 0$  at the origin. The tagged microscopic particle density  $n(r, t)$  leads to the self-part of the van Hove self-density autocorrelation function  $G^s(r, t)$ . The Fourier transform of  $G^s(r, t)$  is the intermediate scattering function:  $F^s(Q, t) = \langle n_Q(t), n_{-Q}(0) \rangle$ . The mean-square displacement evolves linear with time  $\lim_{t \rightarrow \infty} \langle [r(t) - r(0)]^2 \rangle = \langle \Delta r^2(t) \rangle = 6Dt$  for long times. After Fourier transformation the intermediate scattering function becomes a Lorentzian line shape, where the half width at half maximum (HWHM) is directly related to the diffusion coefficient:  $\text{HWHM} = \Gamma = \hbar D Q^2$ . Herein lies the simplicity for a QENS measurement to derive a diffusion

coefficient. That description is correct for long times compared to molecular collisions and describes the random walk of a particle in the picture of Einstein.

A direct connection of the diffusion coefficient with the microscopic particle dynamics can be obtained through a Green-Kubo integral of the velocity autocorrelation function [2]. It became evident that a large part of the microscopic dynamics was not well represented in the Langevin equation, and a generalized Langevin equation was introduced to describe the dynamics [3]. These investigations emphasized the coupling to further fluctuations, which contribute in different strengths to the diffusion process on different length scales. Hence much effort was invested to understand the self-particle dynamics on length scales between the hydrodynamic and the free-streaming length scale to get insight into the microscopic sources for the diffusion process. Within a neutron scattering experiment these length scales can be probed and a deeper analysis through the wave-vector-dependent scattering functions  $F^s(Q, t)$  can be performed.

In general, the classical Gaussian distribution function  $G^s(r, t)$  leads to a Gaussian function in wave vector space [4] for the intermediate scattering function, known as the Gaussian approximation. In the wave vector range between small, hydrodynamic and large, free-particle wave vectors the Gaussian approximation breaks down [3]. Early MD simulations on a Lennard-Jones liquid demonstrated non-Gaussian deviations with increasing wave vector [5]. The study showed a minimum of the reduced halfwidth  $\gamma(Q) = \frac{\Gamma(Q)}{DQ^2}$  around the structure factor peak, where  $\Gamma(Q)$  denotes the HWHM.

To describe the linewidth reduction at intermediate wave vectors a successful approach is to apply sophisticated approximations to the friction force in a generalized Langevin equation for the self-scattering function  $F^s(Q, t)$ . This can be achieved with inclusion of nonlocal effects in time and space through a memory function approach with a single

\*franz.demmel@stfc.ac.uk

exponential decay function for the second order memory function [6]. The incoherent Lovesey model could already demonstrate the experimentally observed linewidth reduction with increasing wave vector in a qualitative manner. Further progress was finally achieved with inclusion of several decay channels into the memory function [7,8]. These approximations were able to describe quantitatively the evolution of the reduced linewidth with increasing wave vector for a dense liquid. When lowering the temperature this reduction in mobility is at the heart of the freezing process and eventually for the glass transition. The most precise tests of these theory predictions have been made on the self-dynamics of liquid sodium. The reduction in width and the derived diffusion coefficient were in excellent agreement with the theory prediction and literature [9–13].

Here we present an investigation of self-diffusion in a binary molten salt. The chosen NaBr has neutron scattering properties where mainly the sodium self-dynamics is observed and methods from the monatomic case can be adopted. The study of molten alkali halides has a long tradition in theory and experiment as well as simulation as documented in reviews and textbooks [2,14,15]. From the application side molten salts are seeing a renaissance. The large heat capacities and large liquid temperature range make molten salts attractive as heat storage and transport media, e.g., for heat storage in modern solar power plants or in next-generation nuclear reactors [16,17].

Structurally, Coulomb liquids exhibit short-range order due to the electrical charges, which are alternating in successive coordination shells around a central ion. The most exciting prediction concerning the dynamics of binary ionic liquids was the existence of optic-type modes, which have been demonstrated in a pioneering MD simulation of a symmetric molten salt by Hansen and McDonald [18]. Due to these predictions in the following years significant experimental effort was put into the study of the collective particle dynamics of molten salts with neutrons [19–21] and with inelastic x-ray scattering [22–27].

On the computational side more effort was devoted to elucidate the microscopic dynamical foundations of transport parameters. First simulations on molten salts used classical rigid ion potentials to derive transport coefficients [28] and are still used nowadays; see, for example, Refs. [29–31]. In parallel, the inclusion of polarization effects was achieved, which resulted in an increase of the diffusion coefficient for the cation [32]. Later, several studies assessed the influence of polarization on the ion dynamics [33–35], and *ab initio* methods also have been applied; see, for example, Refs. [36–38].

Not as many experimental studies exist on the microscopic dynamics, mostly due to the corrosive nature of the sample and the necessary high temperatures. Pulsed field gradient nuclear magnetic resonance spectroscopy has successfully been applied to study structure and ion dynamics [39]. Quasielastic neutron scattering (QENS) is a powerful method to study single-particle dynamics on a microscopic scale and to derive a diffusion coefficient without disturbance from convection. In addition, QENS offers the possibility to study the evolution of single-particle dynamics over decreasing length scales and hence the influence of the microscopic structure on the diffusion process. The determination of a tagged particle

motion needs access to a quantity sensitive to single-particle movements, and incoherent neutron scattering provides exactly this tool.

One of the few examples in this field is a QENS study on sodium movements in molten NaI [40]. More recently, the single-ion dynamics of molten NaBr and NaF was studied in a combination of experiment with classical and first-principles-based MD simulations [33,41–43]. These investigations of the ionic mobility examined the ion self-diffusion coefficients  $D$  and compared the simulated and experimental results with macroscopic diffusion coefficients obtained through tracer diffusion. Until now, to our best knowledge no specific analysis has been undertaken to study the diffusion process with decreasing length scale as was done for monatomic metallic liquids.

Here we present a QENS measurement on molten NaBr just above the melting point with the aim to determine the single-particle motions of the sodium ion with increasing wave vector. Due to the neutron scattering properties of the involved ions the scattered intensity is dominated by the single-particle motions of the sodium ion.

## II. EXPERIMENTAL DETAILS

Inelastic neutron scattering measures the total dynamic structure factor  $S(Q, \omega)$  of the density fluctuations. Non-magnetic neutron scattering interacts with the nuclei through two cross sections, the incoherent and the coherent one. The incoherent cross section connects with the self-correlations of a particle, and the coherent cross section interferes with correlations between the particles. In general, the double differential cross section per particle is a cross-section-weighted sum of these two contributions [19]:

$$\begin{aligned} \frac{d^2\sigma}{d\Omega d\omega} &= \frac{d^2\sigma}{d\Omega d\omega}|_{\text{coh}} + \frac{d^2\sigma}{d\Omega d\omega}|_{\text{inc}} \\ &= \frac{k_f}{k_i} \sum_{i,j} \sqrt{c_i c_j} b_i b_j S_{i,j}(Q, \omega) \\ &\quad + \frac{k_f}{k_i} \sum_i \frac{\sigma_i^{\text{inc}}}{4\pi} c_i S_i^s(Q, \omega). \end{aligned} \quad (2)$$

Here  $k_i$  and  $k_f$  denote the incoming and scattered wave vectors and  $c_i$  are the respective particle concentrations. The coherent double differential cross section is related to a sum of the partial dynamic structure factors  $S_{i,j}(Q, \omega)$  weighted by the square of the respective neutron scattering lengths, and the incoherent one is related to a sum of the self-dynamic structure factors  $S_i^s(Q, \omega)$  weighted by their respective incoherent cross sections. In a binary system, like NaBr, the measured intensity will consist of five different contributions, and the coherent and incoherent dynamic structure factors may be written

$$\begin{aligned} S_{\text{coh}}(Q, \omega) &= \frac{1}{2} [b_{\text{Na}}^2 S_{\text{NaNa}}(Q, \omega) + 2b_{\text{Na}} b_{\text{Br}} S_{\text{NaBr}}(Q, \omega) \\ &\quad + b_{\text{Br}}^2 S_{\text{BrBr}}(Q, \omega)], \end{aligned} \quad (3)$$

$$S^s(Q, \omega) = \frac{1}{2} \left[ \frac{\sigma_{\text{Na}}^{\text{inc}}}{4\pi} S_{\text{Na}}^s(Q, \omega) + \frac{\sigma_{\text{Br}}^{\text{inc}}}{4\pi} S_{\text{Br}}^s(Q, \omega) \right]. \quad (4)$$

TABLE I. Neutron scattering lengths, cross sections, and absorption cross sections.

	$b$ (fm)	$\sigma_a^{\text{coh}}$ (barn)	$\sigma_a^{\text{inc}}$ (barn)	$\sigma_a^{\text{abs}}$ (barn)
Na	3.6	1.66	1.62	0.53
Br	6.795	5.8	0.1	6.9

Table I provides the scattering lengths and the neutron cross sections of both ions [44]. Na is a nucleus with nearly equal coherent and incoherent scattering cross section, and Br scatters the neutrons mainly coherently. Hence the total incoherent scattering cross section is dominated by the sodium movements, and the bromine ions contribute only a few percent to the incoherent scattering. The non-negligible coherent cross section from bromine and sodium ions will contribute to the measured intensity mainly towards the structure factor maximum. However, there is also a non-negligible contribution at smaller  $Q$  vectors which will need to be corrected for to obtain the pure self-dynamics of the molten salt.

A flat niobium can was filled with NaBr powder, which was then enclosed through electron beam welding. The niobium wall thickness was 0.5 mm, and the sample thickness 3.8 mm, which provided a scattering power of about 12%. Niobium is a nearly perfect coherent scatterer and hence will not contribute to the elastic line except where Debye-Scherrer lines appear. The first reflection of niobium is at  $Q = 2.7 \text{ \AA}^{-1}$ , which is outside the wave vector range of the spectrometer setup. The cell was installed under a  $45^\circ$  orientation in a transmission geometry into a standard furnace with niobium shields. The flat cell installed under this geometry gives a high self-absorption at a  $Q \approx 1.6 \text{ \AA}^{-1}$ , which is near the structure factor maximum of molten NaBr. That momentum transfer is outside the region of interest for this experiment. The measured temperature was 1033 K for molten NaBr ( $T_{\text{melt}} = 1000 \text{ K}$ ). The temperature uncertainty was smaller than  $\pm 1.5 \text{ K}$  during all measurements. An identical cell was used for empty cell runs. The experimental density of molten NaBr at  $T = 1033 \text{ K}$  is  $2.34 \text{ g/cm}^3$  [45].

The QENS experiment was performed at the OSIRIS spectrometer of the U.K. ISIS Facility [46]. With an end energy of  $E_f = 1.845 \text{ meV}$  the energy resolution deduced from a vanadium measurement was  $\text{FWHM} = 0.025 \text{ meV}$ , and the covered wave vector range is  $0.25 \text{ \AA}^{-1} < Q < 1.8 \text{ \AA}^{-1}$ . In contrast to the previous measurement [33] a beryllium filter was installed this time on the spectrometer [47] to remove potential contaminations from second-order reflections of the pyrolytic graphite analyser. About 36 hr of beam time were used for the sample and 20 hr for the empty cell measurement to obtain data of high statistical quality [48].

Figure 1 shows an intensity map of molten NaBr at 1033 K. Towards small  $Q$  vectors a strong increase in the amplitude can be observed, a sign of quasielastic incoherent scattering. This shape demonstrates that the measured signal stems from sodium diffusion within this range of  $Q$  vectors. At  $Q$  vectors towards  $Q \approx 1.7 \text{ \AA}^{-1}$  the dynamic structure factor shows a smooth continuous increase in intensity due to coherent scattering.

To determine the small deviations from the hydrodynamic diffusion behavior a quite sophisticated data analysis

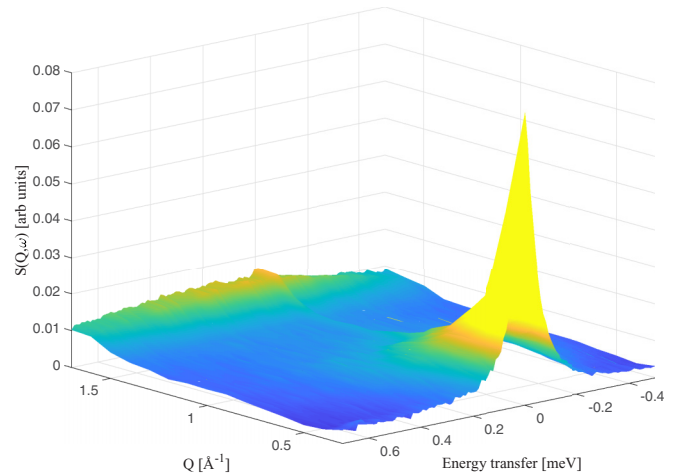


FIG. 1. An intensity map of the measured molten NaBr signal is presented. At small  $Q$  the typical scattering signal of an incoherent scattering particle is visible, and towards larger wave vectors a smooth increase in intensity from the coherent, collective movements of the particles can be seen.

procedure is in order. The data analysis included monitor normalization and empty cell subtraction taking into account absorption of sample and can. Absorption factors have been calculated according to a procedure from Paalman and Pings [49].

Figure 2 shows two sample spectra with the respective empty cell measurement. The empty niobium cell clearly contributes only a small amount to the signal at this wave vector. Included is also the energy resolution ( $\text{FWHM} = 0.025 \text{ meV}$ ), which is for most  $Q$  vectors much smaller than the measured spectra from the molten salt. Through comparison with a vanadium measurement an absolute normalization was achieved. Interpolation on the measured grid of energy momentum transfers enabled the conversion into constant  $Q$  spectra.

In a scattering experiment there exists a finite probability that the once scattered neutron is scattered a second time

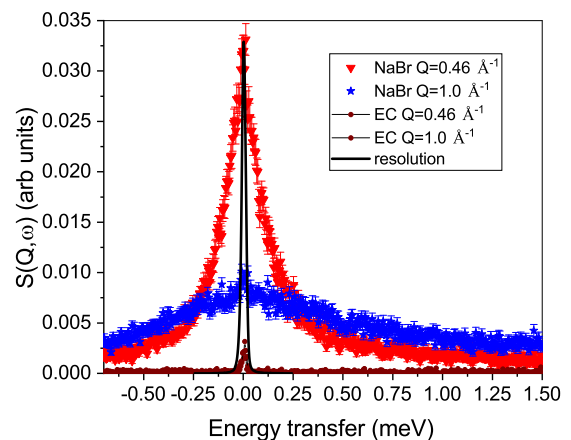


FIG. 2. Two noncorrected measured spectra for two different wave vectors are plotted. Included are the respective empty cell measurements and the measured energy resolution from a vanadium measurement.

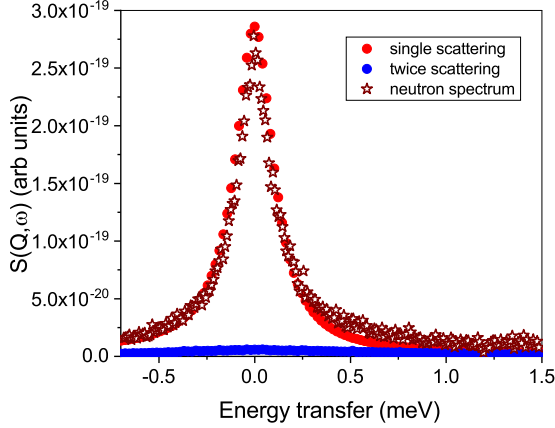


FIG. 3. The single-scattering input signal and the twice-scattered signal are plotted from the multiple-scattering correction calculation. Included (stars) is the measured neutron spectrum at  $Q = 0.475 \text{ \AA}^{-1}$ .

or even more often. The multiple-scattered neutron signal can be calculated from a convolution of the single-scattering function. This convolution process results in much less structured spectra. These unwanted additional scattering events need to be corrected from the measured spectra to extract the single-scattering function. To this end a multiple-scattering correction has been performed. This was achieved by simulation of the twice-scattered neutrons given a suitable scattering function as input and subtracting the twice-scattered neutron intensity from the measured signal [50].

For the calculation of the multiple-scattered signal incoherent and coherent dynamic structure factors are needed as input. As an approximation the dynamic structure factors were used derived from a single exponential decaying memory function ansatz [2]. That model delivers a dynamic scattering function for the collective and for the self-dynamics of a liquid. This so-called viscoelastic model describes the collective dynamics reasonably well, which was recently demonstrated in a data analysis of the collective dynamics of molten RbBr [21]. Also the incoherent model was successfully applied in the description of self-dynamics in monatomic liquids [6]. An important input parameter for the calculation of the dynamic structure factor is the Einstein frequency, which can be estimated from the Debye temperature, which is  $\theta_D = 224 \text{ K}$  for NaBr [51]. An estimate for  $\omega_E$  can then be calculated with  $\omega_E = \frac{3}{4}\omega_D$ , from which we finally obtain  $\omega_E = 23 \times 10^{12} \text{ s}^{-1}$ .

After proper normalization with the experimental absolute normalized data the twice-scattered contribution was subtracted from the data. In Fig. 3 the input scattering function and the simulated twice-scattered contribution are plotted compared with the measured data for a  $Q$  vector of  $Q = 0.475 \text{ \AA}^{-1}$ . The line shape is well described by the viscoelastic model, and the integrated contribution from the twice-scattered neutrons is around 7% at this wave vector in comparison to the single-scattered neutron signal.

A further step is necessary to obtain the pure self-dynamics, the non-negligible contribution from the collective motions has to be subtracted. To achieve this a MD-simulated spectrum for the collective motions  $S_{\text{coh}}(Q, \omega)$  has

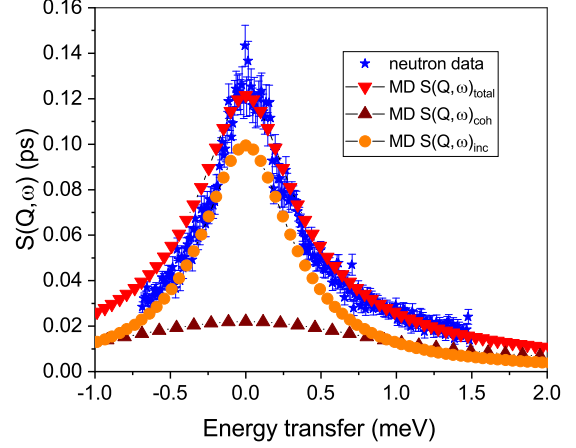


FIG. 4. A measured spectrum at  $Q = 0.85 \text{ \AA}^{-1}$  is plotted with MD-simulated spectra for the incoherent, the coherent, and the total  $S(Q, \omega)$ .

been subtracted from the experimental spectra. A good absolute calibration of the data is mandatory for a successful application of this correction. In Fig. 4 the neutron spectrum at  $Q = 0.85 \text{ \AA}^{-1}$  is plotted after multiple-scattering correction and absolute calibration. Included are the results from the MD simulation [41] for  $Q = 0.82 \text{ \AA}^{-1}$  depicting the total, the incoherent, and the coherent contribution.

In this wave vector range the coherent amplitude at the elastic line is only 20% of the incoherent one. The coherent spectrum is wider and demonstrates a sizable amount to the total signal for energy transfers beyond 0.7 meV. There is a very good agreement on an absolute intensity scale, which gives confidence in subtracting the simulated coherent signal from the neutron data. For the smooth  $Q$  dependence of  $S_{\text{coh}}(Q, \omega)$  the line shape of the simulated spectrum at  $Q = 0.82 \text{ \AA}^{-1}$  has been normalized with the simulated total structure factor data, obtained from the partial structure factors [41]. To extract the linewidth  $\Gamma(Q)$  a Lorentzian convoluted with the measured resolution function was fitted to the spectra, even though only at the smallest momentum transfer would the convolution make a small difference. No additional background was included in the fit procedure. All details from the MD simulation have been published before and are for the sake of brevity not repeated here [33,41].

### III. RESULTS AND DISCUSSION

#### A. Diffusion on long length scales

First we will describe the line shape with two different methods to derive the sodium diffusion coefficient before we embark on discussing the changes of  $D$  with increasing wave number. A formal framework to describe the dynamics of time correlation functions is given by the Zwanzig-Mori memory function formalism. Within a generalized Langevin equation all processes contributing to the time development of the correlation function are buried in the space- and time-dependent memory function. A solution to this integro-differential equation can be obtained through a Laplace transform into a continued fraction.

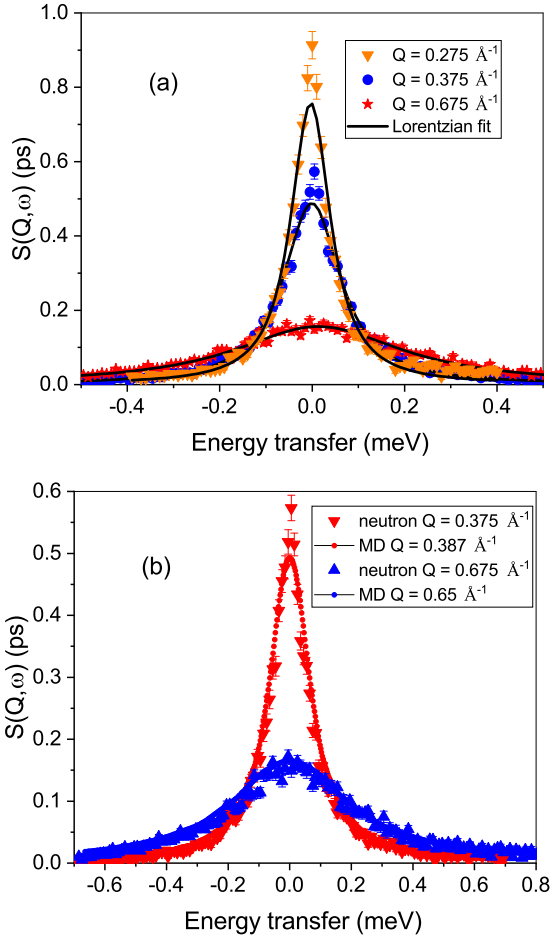


FIG. 5. Fully corrected spectra for three wave vectors are plotted in panel (a) together with their respective Lorentzian line-shape fit. In panel (b) a comparison is made between the simulated and experimental spectra for two wave vectors.

From hydrodynamics a Lorentzian line shape is predicted, and that is the standard fit model to extract the diffusive motions in liquids. In a formal description the Lorentzian line shape can be derived from a memory function approximation with an instantaneously decaying first-order memory function  $K(Q, t) = 2\Gamma\delta(t)$  [4]. The Laplace transformed Langevin equation for the self-density autocorrelation function is then

$$F^s(Q, z = i\omega) = \frac{1}{z + K(Q)}. \quad (5)$$

The real part of  $F^s(Q, z)$  is related to the single-particle scattering function through  $S^s(Q, \omega) = \frac{1}{\pi}\text{Re}(F^s(Q, z))$ , which is in this case a Lorentzian.

After performing all the necessary data evaluation steps we obtain the pure  $S^s(Q, \omega)$ , which is mostly related to the sodium movements. Figure 5(a) depicts three spectra with different  $Q$  vectors and their respective fit of a Lorentzian. The larger  $Q$  vector is described perfectly by a one-Lorentzian fit. However, at  $Q$  values smaller than  $Q < 0.575 \text{ \AA}^{-1}$  the amplitude is not perfectly fitted by a single Lorentzian function. Figure 5(b) shows two neutron spectra compared with the MD-simulated spectra. There is an excellent agreement

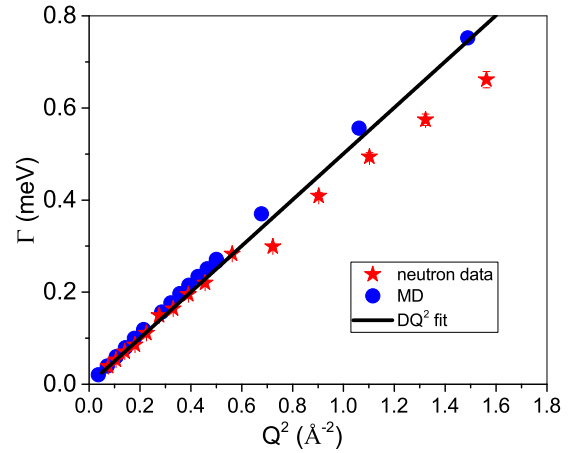


FIG. 6. The widths from the experimental and MD-simulated data are plotted against  $Q^2$ . The line depicts a  $DQ^2$  fit to the neutron data for a wave vector range with  $Q^2 < 0.3 \text{ \AA}^{-2}$ .

on line shape and intensity scale, except that at the smaller wave vector the experiment shows a larger amplitude. Reasons for the enhanced amplitude could be a not well subtracted empty cell or an additional slow process. At larger  $Q$  vectors the empty cell subtraction worked quite well, and the small amount from the empty cell (see Fig. 2) does not change very much with increasing wave vector. On the other side the enhanced intensity could be seen as an additional slow process which appears on top of the salt dynamics. There is a small incoherent contribution from the larger bromine ions. However, the MD simulation predicted a 25% reduction in the diffusion coefficient compared to  $D_{\text{Na}}$  [33]. A fit with two Lorentzians indicated a factor 2 smaller width for the additional slower contribution. Hence it seems difficult to explain this additional intensity with the bromine self-movements. Also the simulated spectrum in Fig. 5(b) contains the contributions from sodium and bromine ions and does not describe this additional intensity. Another explanation could be that the self-diffusion process is a more complex process than only a single exponentially decaying intermediate self-scattering function.

The derived widths  $\Gamma(Q)$  from the fit procedure are plotted in Fig. 6. For comparison the widths from the MD-simulation spectra are included, which have been obtained from the Fourier transformed total self-intermediate scattering function  $F^s(Q, t)$  [33]. At small wave vectors there is a good agreement, whereas at larger  $Q$  vectors the experimental data lie slightly below the simulated results. With a fit of the hydrodynamic diffusion law  $\Gamma = \hbar D Q^2$  in the small wave vector range up to  $Q^2 = 0.3 \text{ \AA}^{-2}$  a diffusion coefficient was extracted from both data sets. The line in the plot indicates the  $DQ^2$  fit to the neutron data, which was then extrapolated to larger  $Q$  values. It clearly indicates that at larger wave vectors the linewidth is reduced compared to the hydrodynamically expected value. A similar behavior could be shown for the MD-simulated results. From the fit we obtain  $D_{\text{Na}} = 7.6 \pm 0.15 \times 10^{-5} \text{ cm}^2/\text{s}$  and from the MD simulation  $D_{\text{Na}} = 8.4 \times 10^{-5} \text{ cm}^2/\text{s}$ . Compared to the previous analysis [33] the experimental derived diffusion coefficient is smaller. This is expected due to the more detailed analysis where further

contributions to the measured signal have been subtracted to obtain the pure incoherent signal. The analysis here then suggests that the simulation slightly overestimates the mobility of the ions, which might be related to an overestimated polarization contribution in the potential description of the bromine ion.

A more sophisticated model to describe the line shape of a tagged particle scattering function was proposed by Lovesey for a monatomic liquid [6]. Within a memory function approach the influence of density fluctuations of the surrounding particles on the tagged particle movements is taken into account by using a second-order memory function [2,4]:

$$F^s(Q, z = i\omega) = \frac{1}{z + \frac{\omega_s^2(Q)}{z + M(Q, z)}}. \quad (6)$$

Here  $\omega_s^2 = \frac{k_B T}{m} Q^2$  is the second frequency moment of the scattering function,  $k_B$  is the Boltzmann constant,  $T$  is the temperature, and  $m$  is the particle mass. Due to the size of the neutron cross sections the main part of the incoherent scattered intensity stems from the sodium ion movements. Hence, we adopt the single-particle scattering function for the binary molten alkali halide. For the memory function an exponentially decaying function is applied:  $M(Q, t) = M(Q, 0) \exp[-t/\tau(Q)]$ . The resulting single-particle scattering function  $S^s(Q, \omega)$  can then be written as

$$S^s(Q, \omega) = \frac{1}{\pi} \frac{\tau(Q) \omega_s^2 (2\omega_s^2 - \omega_E^2)}{\omega^2 \tau(Q)^2 (\omega^2 - 3\omega_s^2 - \omega_E^2)^2 + (\omega^2 - \omega_s^2)^2} \quad (7)$$

with  $\omega_E$  as the Einstein frequency of the liquid. For the relaxation time  $\tau(Q)$  of the memory function a recipe was proposed which fulfills the low- $Q$  hydrodynamic limit [6]:

$$\frac{1}{\tau(Q)} = \frac{Dm\omega_E}{k_B T} \sqrt{2\omega_s^2 + \omega_E^2}. \quad (8)$$

With the Einstein frequency of  $\omega_E = 23 \times 10^{12} \text{ s}^{-1}$  as input parameter and all the other parameters given, a wave-vector-dependent diffusion coefficient  $D(Q)$  can be obtained. Figure 7 shows examples for the measured spectra and the respective fit with Eq. (7). The inset shows the spectra on a linear scale and still demonstrates a small missing part at the smallest  $Q$  vector, similar to the observation with the Lorentzian curve fit. From the fit over all  $Q$  vectors we obtain wave-vector-dependent diffusion coefficients  $D(Q)$ . Figure 8 depicts the obtained  $D(Q)$  values from the curve fitting with the Lorentz line shape and the Lovesey model. The values from the Lorentz fit deviate with increasing wave vector from the hydrodynamic expected value, as expected from the width plot in Fig. 6. However, the fit with the Lovesey model delivers  $D(Q)$  values nearly independent of the wave vector. Clearly this model takes some feedback of the surrounding particles through the time-dependent memory function into account. Included in the figure are fits to the diffusion coefficients  $D(Q)$ . A quadratic decay for  $D(Q)$  in the case of the Lorentzian curve fit and a constant  $D$  value for the Lovesey curve fits was applied to the  $D(Q)$  values in Fig. 8. The motivation for the quadratic fit will be presented below.

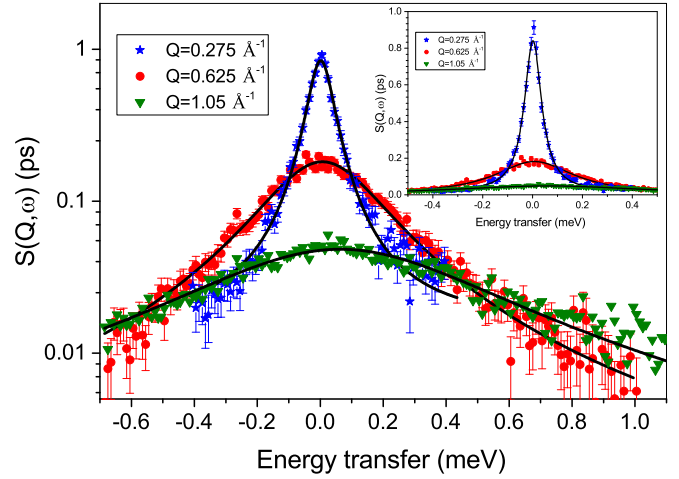


FIG. 7. Spectra for three different  $Q$  vectors are presented on a logarithmic scale. The lines depict fits with the incoherent Lovesey model. The inset shows the spectra on a linear scale to emphasize the difference between fit and data at the smallest wave vector.

The hydrodynamic limit  $Q \rightarrow 0$  defines the diffusion coefficient. The quadratic fit delivers  $D_{\text{Na}} = 7.78 \pm 0.23 \cdot 10^{-5} \text{ cm}^2/\text{s}$  and the  $Q$  constant fit  $D_{\text{Na}} = 7.78 \pm 0.1 \cdot 10^{-5} \text{ cm}^2/\text{s}$ . That perfect agreement might be by chance or be evidence for the consistent data analysis procedure. Within error bars these values agree with the value derived from the  $\Gamma(Q)$  fit. The slightly different value for the diffusion coefficient obtained through the  $Q^2$  fit can then be understood as reasoned by the deviation from Fick's diffusion law with increasing wave vector. Herein lies also a possible source for observed deviations in reported diffusion coefficients, because the actual value of  $D$  depends on the fitting range of available wave vectors. We conclude from the analysis based on two different analysis methods that the experimental value for the sodium ion diffusion coefficient in molten NaBr is  $D_{\text{Na}} = 7.8 \pm 0.2 \times 10^{-5} \text{ cm}^2/\text{s}$ .

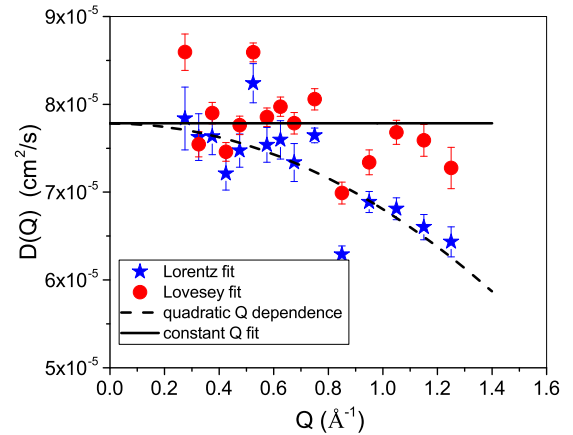


FIG. 8. The wave-vector-dependent diffusion coefficients  $D(Q)$  are presented, derived from the two analysis procedures using a Lorentzian spectral shape (stars) and a fit with the Lovesey model (circles). Included are fits with a quadratic  $Q$  behavior (dashed line) and a constant  $D$  fit (line) through the respective data sets.

Now we aim to describe the obtained diffusion coefficient with a simple theoretical model based on collisions of hard spheres. Kinetic theory has been used to describe transport coefficients of dense fluids. Originally Enskog proposed a generalization of the Boltzmann equation for a gas of hard spheres by taking into account the local density and only binary collisions. Later the Enskog theory was further developed to be applied for binary mixtures of hard spheres; see, for example, [52–54]. An Enskog expression for the self-diffusion coefficient  $D_E$  of binary and multicomponent mixtures of hard spheres was given previously [55,56]:

$$D_{E,1} = \frac{3k_B T}{16\pi} \left\{ \sigma_1^2 n_1 g_{11}(\sigma_1) \sqrt{\frac{k_B T m_1}{4\pi}} + \sigma_{12}^2 n_2 g_{12}(\sigma_{12}) \sqrt{\frac{k_B T m_1 m_2}{2\pi(m_1 + m_2)}} \right\}^{-1}. \quad (9)$$

Here  $T$  denotes the temperature,  $m_1$  and  $m_2$  are the masses of the particles, and  $n_{1,2}$  are the particle densities of the two ions. The hard-sphere diameters for the ions  $\sigma_{\text{Na}} = 1.9 \text{ \AA}$  and  $\sigma_{\text{Br}} = 3.9 \text{ \AA}$  are taken from Ref. [45]. For the unlike particle interaction  $\sigma_{12} = (\sigma_1 + \sigma_2)/2$  is applied. The remaining parameters to be determined are the pair distribution functions at contact  $g_{ij}(\sigma_{ij})$ . For mixtures of hard spheres a solution for the Percus-Yevick equation was given by Lebowitz [57]:

$$g_{11}(\sigma_1) = \frac{(1 + \frac{1}{2}\zeta) + \frac{3}{2}\eta_2\sigma_2^2(\sigma_1 - \sigma_2)}{(1 - \zeta)^2} g_{12}(\sigma_{12}) = \frac{\sigma_2 g_{11}(\sigma_1) + \sigma_1 g_{22}(\sigma_2)}{2\sigma_{12}}. \quad (10)$$

The packing fraction for the binary mixture is given by  $\zeta = \eta_1\sigma_1^3 + \eta_2\sigma_2^3$  with  $\eta_i = \frac{\pi}{6}n_i$ . We obtain  $\zeta = 0.47$  for molten NaBr, which is near the solidification packing fraction of a dense hard-sphere liquid. For this Enskog approximation we obtain the following self-diffusion coefficients:  $D_{E,\text{Na}} = 18 \times 10^{-5} \text{ cm}^2/\text{s}$  and  $D_{E,\text{Br}} = 5.6 \times 10^{-5} \text{ cm}^2/\text{s}$ . The Enskog diffusion coefficient for the sodium ions is about a factor 2 larger than the measured and simulated one, whereas the bromine diffusion coefficient is about the simulated one,  $D_{\text{Br}} = 5.8 \times 10^{-5} \text{ cm}^2/\text{s}$  [33]. The sodium ions are a factor 2 smaller in diameter and a factor 4 lighter than the bromine particles, which explains the large difference in the hard-sphere Enskog calculation for the diffusion coefficient. The small hard-sphere particles are surrounded by a mixture of small and large particles and can more easily find a free space to move randomly around than the large particles. On the other side the large bromine spheres are hindered in their movements only by their own species, which might explain the good agreement between the hard-sphere Enskog result for  $D_{\text{Br}}$  with the simulated diffusion coefficient. An experimental determination of the bromine diffusion coefficient based on a hard-sphere theory was able to predict  $D_{\text{Br}}$  quite well [41]. The difference with the Enskog diffusion constant obtained there might be related to two different implementations for structural influences into the kinetic theory. In summary, there is a mixed success to predict diffusion coefficients for molten salts applying hard-sphere kinetic theories.

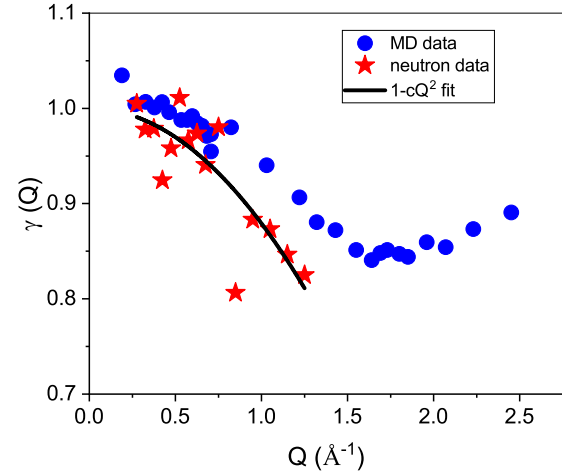


FIG. 9. The reduced widths are plotted for the neutron data (stars) and the MD-simulation data (circles). Included as a line is a fit with a quadratic wave vector dependence of the reduced width.

For liquid alkali metals it was shown that diffusion coefficients, taking into account only binary collisions, are about 50% larger than the experimental or simulated ones [9]. Within that context the large value for  $D_{\text{Na}}$ , based on only binary collisions of hard spheres, might be partly explained by the neglect of slow decay processes of the memory function.

### B. Diffusion with increasing wave vector

Near the melting point the diffusion process in the dense liquid is hindered by density fluctuations, and it appears that this principle also applies for the binary ionic liquid. Whether the coupling to density fluctuations is the dominating variable behind the changes to the self-diffusion coefficient in a molten salt will now be examined in more detail by means of the wave-vector-dependent diffusion.

Formally it is necessary to extend the space and time dependence in the memory function  $M(Q, t)$  beyond the phenomenological ansatz in the Lovesey model. That can be achieved by splitting the memory function into a fast-decaying and a slow-decaying part  $M(Q, t) = M^{\text{fast}}(Q, t) + M^{\text{slow}}(Q, t)$  [4]. The latter contribution is related to density and current fluctuations of the system, which is the reason for the term mode coupling approach. Then the dynamic equation for the correlation function can be solved in a self-consistent way under the assumption for a specific set of modes within the memory function. For the incoherent scattering function of a classical liquid such an approach was undertaken using density and current fluctuations [7]. In the dense liquid a quadratic decrease at small wave vectors was predicted by theory [7] and was later confirmed in pioneering experiments on liquid sodium [11,12]:

$$\gamma(Q) = 1 - cQ^2. \quad (11)$$

The constant  $c$  is related to the memory function of the kinetic equation for the tagged particle phase-space correlation function [7]. In particular, the constant depends on the long time development of the memory function.

In Fig. 9 the reduced widths  $\gamma(Q) = \frac{\Gamma(Q)}{\hbar D Q^2}$  for the neutron data and the MD-simulation data are plotted, using the respec-

tive diffusion coefficients. Beyond a wave vector of about  $Q \approx 0.5 \text{ \AA}^{-1}$  the reduced width deviates from the expected hydrodynamic value towards smaller values.  $D(Q)$  decreases with increasing wave vector when the diffusing particle senses the atomic structure. The neutron data show a larger degree of statistics, but, nevertheless, they also demonstrate the decrease in the reduced width in reasonable agreement with the MD simulation. MD-simulation data are available beyond the first structure factor maximum at  $Q = 1.7 \text{ \AA}^{-1}$ . The simulation results indicate a minimum for  $\gamma(Q)$  with an increase beyond the structure factor maximum. Theory predicted a so-called cutoff wave vector  $Q^* = \frac{\omega_E}{2\sqrt{k_B T/m}}$  when the minimum occurs for  $\gamma(Q)$  [8]. Here we calculate for the sodium ions a  $Q^* = 1.88 \text{ \AA}^{-1}$ , which agrees quite well with the minimum in the simulation data. That  $Q$  dependence agrees with the behavior in monatomic liquids [13], where the minimum is interpreted that the particle is trapped inside the cage of next neighbors. At even shorter distances or larger wave vectors the particle does not feel the influence of the surrounding neighbors. Theory and simulations have shown that beyond about twice the structure factor maximum there is a dramatic change of the reduced width toward the free particle behavior [8,13]. That wave vector range has not been reached in the MD simulation.

To test these predictions a linear and a quadratic fit to the experimental data were performed, and the quadratic fit shows a smaller  $\chi^2$ . Applying the quadratic fit of Eq. (11) to the neutron data we obtain  $c = 0.12 \pm 0.015 \text{ \AA}^2$  and for the MD data  $c = 0.06 \pm 0.004 \text{ \AA}^2$  is derived. For liquid sodium near the melting point  $c = 0.074 \text{ \AA}^2$  was obtained [58]. An estimate for the constant  $c$  can be derived using the incoherent Lovesey model [see Eq. (7)]. For small  $Q$  the reduced width for the incoherent Lovesey model was given in Ref. [4], which can be expanded to demonstrate a  $Q^2$  dependence:

$$\gamma(Q) = \left[ 1 + \frac{2k_B T}{m\omega_E^2} Q^2 \right]^{-1/2} \approx 1 - \left[ \frac{k_B T}{m\omega_E^2} \right] Q^2. \quad (12)$$

Using the above estimated Einstein frequency  $\omega_E = 23 \times 10^{12} \text{ s}^{-1}$  we obtain  $c = 0.07 \text{ \AA}^2$ . A more elaborate derivation for the small  $Q$  dependence of the reduced width, which was successfully applied in the case of liquid sodium, was presented in Ref. [58]:

$$\gamma(Q) = 1 - \left[ \frac{2k_B T}{m\omega_E^2} - \frac{D^2 m}{k_B T} \right] Q^2. \quad (13)$$

That approximation delivers a  $c = 0.12 \text{ \AA}^2$  in our case, in excellent agreement with the experimental result. The good agreement between calculated curvature and fitted value suggests that the same processes are at work in the molten salt as in the monatomic liquid metal sodium. In liquid sodium the quadratic dependence was linked to the coupling to density fluctuations [11]. Therefore the quadratic decrease in molten NaBr near the melting point is evidence for a coupling to density fluctuations, which are hindering the diffusion process with decreasing length scale.

It seems conceivable that at higher temperature and concomitant lower density the cage effect dies away and the coupling to transverse currents takes over. Consequently changes in the  $Q$  dependence of the reduced width and to the diffusion

coefficient could be expected in a molten salt, as demonstrated for liquid sodium [11,12,59].

#### IV. CONCLUSIONS

A quasielastic neutron scattering experiment on molten NaBr just above the melting point was conducted. A quite detailed data analysis was performed to reveal the pure self-dynamics of the molten salt. To this end a multiple-scattering correction was undertaken, and the simulated coherent scattering contribution was subtracted from the absolute calibrated data. A good agreement with simulated data was achieved concerning the obtained spectra and their linewidths. Two methods have been applied to determine the hydrodynamic diffusion coefficient, and both approaches demonstrate a remarkable agreement for the long length scale movements. A simple calculation for the diffusion coefficient based on binary collisions of hard spheres fails to describe the sodium diffusion coefficient. However, the larger and heavier bromine seems to be described quite well.

The resulting reduced width demonstrates a quadratic decrease with increasing  $Q$  vector in the experimental and simulated data at small wave vectors. The decrease in  $D(Q)$  with decreasing length scale is caused by the influence of the microscopic structure of the dense liquid. As a consequence the cage from the surrounding particles hinders the particle's diffusion movements. This  $Q$  dependent behavior might be interpreted as a coupling of the diffusion process to density fluctuations. In monatomic liquid metals such an explanation could be demonstrated quantitatively with mode coupling theory calculations. The presented results suggest a similar mechanism in molten NaBr.

However, some questions remain. Towards small  $Q$  vectors the experimental spectra demonstrate an additional slow process, which is not seen in the simulation. Further experimental and MD-simulation studies are necessary to confirm or refute the existence of an additional slow relaxation process. To access the minimum in the reduced width experimentally a possibility would be to perform a QENS experiment with polarization analysis. Also it would be interesting to watch the evolution of the reduced width with increasing wave vector in simulation and experiment towards the free particle limit. A much more demanding challenge for the experiment would be to follow the diffusion process towards lower density and to reveal the changes in the coupling to decay channels of the memory function. Certainly a simulation could achieve these thermodynamic conditions more easily under the condition that a reliable interaction potential with the changing density is available. And finally from the theoretical point of view, a calculation of the  $Q$ -dependent  $\gamma(Q)$  decrease for a binary Coulomb liquid could give new impulses to the field.

#### ACKNOWLEDGMENTS

The author is indebted to Christoph Morkel for stimulating discussions and a critical reading of the manuscript. Gratefully acknowledged is the ISIS furnace section for their excellent support. The author thanks O. Alcaraz and J. Trullas for the continuous support from the simulation side. This work was supported by the Science and Technology Facilities Council, STFC.

- [1] H. J. V. Tyrrell and K. R. Harris, *Diffusion in Liquids* (Butterworths, London, 1984).
- [2] J. P. Hansen and I. McDonald, *Theory of Simple Liquids* (Academic Press, London, 2006).
- [3] J. P. Boon and S. Yip, *Molecular Hydrodynamics* (McGraw Hill, New York, 1980).
- [4] U. Balucani and M. Zoppi, *Dynamics of the Liquid State* (Clarendon Press, Oxford, 1994).
- [5] D. Levesque and L. Verlet, *Phys. Rev. A* **2**, 2514 (1970).
- [6] S. W. Lovesey, *J. Phys. C* **6**, 1856 (1973).
- [7] G. Wahnstrom and L. Sjogren, *J. Phys. C: Solid State Phys.* **15**, 401 (1982).
- [8] W. Götze and A. Zippelius, *Phys. Rev. A* **14**, 1842 (1976).
- [9] U. Balucani, A. Torcini, and R. Vallauri, *Phys. Rev. A* **46**, 2159 (1992); *Phys. Rev. B* **47**, 3011 (1993).
- [10] C. Morkel and W. Gläser, *Phys. Rev. A* **33**, 3383 (1986).
- [11] C. Morkel and W.-C. Pilgrim, *J. Non-Cryst.* **312–314**, 128 (2002).
- [12] W.-C. Pilgrim and C. Morkel, *J. Phys.: Condens Matter* **18**, R585 (2006).
- [13] U. Balucani, A. Torcini, A. Stangl, and C. Morkel, *Phys. Scr.* **T57**, 13 (1995).
- [14] N. H. March and M. P. Tosi, *Coulomb Liquids* (Academic Press, San Diego, 1984).
- [15] M. Rovere and M. P. Tosi, *Rep. Prog. Phys.* **49**, 1001 (1986).
- [16] C. LeBrun, *J. Nucl. Mater.* **360**, 1 (2007).
- [17] L. C. Dewan, C. Simon, P. A. Madden, L. Hobbs, and M. Salanne, *J. Nucl. Mater.* **434**, 322 (2013).
- [18] J. P. Hansen and I. R. McDonald, *Phys. Rev. A* **11**, 2111 (1975).
- [19] D. L. Price and J. R. D. Copley, *Phys. Rev. A* **11**, 2124 (1975).
- [20] R. L. McGreevy, *Solid State Phys.* **40**, 247 (1987).
- [21] F. Demmel, D. Szubrin, W. C. Pilgrim, A. De Francesco, and F. Formisano, *Phys. Rev. E* **92**, 012307 (2015).
- [22] F. Demmel, S. Hosokawa, M. Lorenzen, and W.-C. Pilgrim, *Phys. Rev. B* **69**, 012203 (2004).
- [23] F. Demmel, S. Hosokawa, W.-C. Pilgrim, and S. Tsutsui, *Nucl. Instrum. Meth. B* **238**, 98 (2005).
- [24] M. Inui, S. Hosokawa, Y. Kajihara, K. Matsuda, S. Tsutsui, and A. Q. R. Baron, *J. Phys.: Condens. Matter* **19**, 466110 (2007).
- [25] F. Demmel, S. Hosokawa, and W.-C. Pilgrim, *J. Alloys Comp.* **452**, 143 (2008).
- [26] S. Hosokawa, F. Demmel, W.-C. Pilgrim, M. Inui, S. Tsutsui, and A. Baron, *Electrochemistry* **77**, 608 (2009).
- [27] S. Hosokawa, M. Inui, T. Bryk, I. Mryglod, W.-C. Pilgrim, Y. Kajihara, K. Matsuda, Y. Ohmasa, and S. Tsutsui, *Condens. Matter Phys.* **22**, 43602 (2019).
- [28] G. Ciccotti, G. Jacucci, and I. R. McDonald, *Phys. Rev. A* **13**, 426 (1976).
- [29] J. Trullas and J. A. Padro, *Phys. Rev. B* **55**, 12210 (1997).
- [30] J. Wang, J. Wu, Z. Sun, G. Lu, and J. Yu, *J. Mol. Liquid* **209**, 498 (2015).
- [31] R. Brookes, A. Davies, G. Ketwaroo, and P. A. Madden, *J. Phys. Chem. B* **109**, 6485 (2005).
- [32] G. Jacucci, I. R. McDonald, and A. Rahman, *Phys. Rev. A* **13**, 1581 (1976).
- [33] O. Alcaraz, F. Demmel, and J. Trullas, *J. Chem. Phys.* **141**, 244508 (2014).
- [34] M. Dixon, *Philos. Mag.* **B 47**, 509 (1983).
- [35] M. Wilson and P. A. Madden, *J. Phys: Condens. Matter* **6**, A151 (1994).
- [36] G. Tabacchi, C. J. Mundy, J. Hutter, and M. Parrinello, *J. Chem. Phys.* **117**, 1416 (2002).
- [37] N. Galamba and B. J. Costa Cabral, *J. Chem. Phys.* **126**, 024502 (2007).
- [38] M. Salanne and P. A. Madden, *Mol. Phys.* **109**, 2299 (2011).
- [39] M. Leveques, V. Sarou-Kanian, M. Salanne, M. Gobet, M. Groult, C. Bessada, P. A. Madden, and A. Rollet, *J. Chem. Phys.* **138**, 184503 (2013).
- [40] R. L. McGreevy, E. W. J. Mitchell, and F. M. A. Margaca, *J. Phys. C* **17**, 775 (1984).
- [41] F. Demmel, O. Alcaraz, and J. Trullas, *Phys. Rev. E* **93**, 042604 (2016).
- [42] F. Demmel and S. Mukhopadhyay, *J. Chem. Phys.* **144**, 014503 (2016).
- [43] S. Mukhopadhyay and F. Demmel, *AIP Conf. Proc.* **1969**, 030001 (2018).
- [44] V. F. Sears, *Neutron News* **3**, 26 (1992).
- [45] G. J. Janz, *Molten Salts Handbook* (Academic Press, New York, 1967).
- [46] M. T. F. Telling and K. H. Andersen, *Phys. Chem. Chem. Phys.* **7**, 1255 (2005); F. Demmel and K. Pokhilchuk, *Nucl. Instrum. Meth. A* **767**, 426 (2014).
- [47] F. Demmel, D. McPhail, J. Crawford, D. Maxwell, K. Pokhilchuk, V. Garcia-Sakai, S. Mukhopadhyay, M. T. F. Telling, F. J. Bermejo, N. T. Skipper, and F. Fernandez-Alonso, *EPJ Web Conf.* **83**, 03003 (2015).
- [48] F. Demmel, Density dependent deviations from hydrodynamic diffusion in a molten salt (STFC ISIS Neutron and Muon Source, 2017), <https://doi.org/10.5286/ISIS.E.90071193>.
- [49] H. H. Paalman and C. J. Pings, *J. Appl. Phys.* **33**, 2635 (1962).
- [50] F. Demmel, A. Diepold, H. Aschauer, and C. Morkel, *Phys. Rev. B* **73**, 104207 (2006); F. Demmel, D. Pasqualini, and C. Morkel, *ibid.* **74**, 184207 (2006).
- [51] N. W. Ashcroft and N. D. Mermin, *Solid State Physics* (Holt Saunders, Philadelphia, 1976).
- [52] M. K. Tham and K. E. Gubbins, *J. Chem. Phys.* **55**, 268 (1971).
- [53] M. Lopez de Haro, E. G. D. Cohen, and J. M. Kincaid, *J. Chem. Phys.* **78**, 2746 (1983).
- [54] J. M. Kincaid, M. Lopez de Haro, and E. G. D. Cohen, *J. Chem. Phys.* **79**, 4509 (1983).
- [55] H. M. Schaink and C. Hoheisel, *Phys. Rev. A* **45**, 8559 (1992).
- [56] G. Jacucci and I. McDonald, *Physica A* **80**, 607 (1975).
- [57] J. L. Lebowitz, *Phys. Rev.* **133**, A895 (1964).
- [58] A. Stangl, Ph.D. thesis, TU München, 1993.
- [59] W. Montfrooy, I. de Schepper, J. Bosse, W. Glaser, and Ch. Morkel, *Phys. Rev. A* **33**, 1405 (1986).